A Robust Adaptive Iterative Learning Control for Trajectory Tracking of Permanent-Magnet Spherical Actuator

Liang Zhang, Weihai Chen, *Member, IEEE*, Jingmeng Liu, and Changyun Wen, *Fellow, IEEE*

***Abstract*—This paper presents a robust adaptive iterative learning control (ILC) algorithm for 3-DOF permanent magnet (PM) spherical actuators to improve their trajectory tracking performance. The dynamic model of a PM spherical actuator is a multivariable nonlinear system with interaxis coupling terms. Uncertainties such as modeling errors, loads, and external disturbances exist in the model unavoidably, which will affect the performance, including the precision of the control system. Hence, to compensate for these uncertainties, a new hybrid control scheme that consists of a proportional–derivative (PD) feedback control with varying gains, a PD-type ILC with adjustable gains, and a robust term is developed. The new control law combines the advantages of simplicity and easy design of the PD control, the effectiveness of the ILC to handle model uncertainties and repetitive disturbances, and the robustness of the robust term to random disturbances. In addition, to expedite the convergence rate, the gains in the PD feedback control and the PD-type ILC are adaptively adjusted according to the iteration times. It is shown that the system tracking error approaches zero as the number of iterations increases. To demonstrate the proposed algorithm and verify the established theoretical results, both simulations and experiments are conducted. The results have shown that the proposed control algorithm can effectively compensate for various uncertainties and can thus improve the trajectory tracking performance of spherical actuators.**

***Index Terms*—Adaptive control, iterative learning control (ILC), permanent-magnet (PM) spherical actuator, trajectory tracking.**

I. Introduction

SPHERICAL actuators can produce 3-DOF rotational motions in one joint. Compared with conventional 3-DOF actuators that are realized by combining several single-axis motors, 3-DOF spherical actuators have advantages such as a compact structure, no backlash, and a low inertia moment. Therefore, it has wide potential applications in situations where multiple-DOF motions are needed, such as robot manipulators, precision assembling, manufacturing, and automation technology [1], [2].

Research on spherical actuators has been actively carried out for several decades. So far, spherical actuators with various structures and operating principles have been proposed. In this paper, we focus on a permanent magnet (PM) spherical actuator since it has the advantages of a simple structure, a high flux density, and a rapid response [3]. The applications of a PM spherical actuator in industrial areas, including robotics, assembling, and manufacturing, always require high trajectory tracking accuracy. Therefore, to achieve the high performance of a spherical actuator, many control methods have been developed for PM spherical actuators. One typical example is to use the proportional–derivative (PD) control law [4]–[6]. The PD control has the advantages of simplicity in design and implementation. It is known that a PD controller can get acceptable tracking performance for many applications with appropriate control gains. However, the dynamic model of a PM spherical actuator includes nonlinearities, and it has some uncertainties including load variations, modeling errors, frictions, and electromagnetic and other external disturbances [3]. Without suitable compensation for these modeling uncertainties and external disturbances, the trajectory tracking performance of the PD control scheme will be seriously affected. In [7] and [8], a computed torque control method was used to the control of a PM spherical actuator. It is a model-based controller that linearizes and decouples the nonlinear dynamics of a PM spherical actuator. Since dynamic modeling errors cannot be avoided due to both structural and nonstructural uncertainties, the computed torque control method cannot achieve good trajectory tracking performance, particularly in the presence of frictions and other external disturbances. To solve these problems, neural networks (NNs) are also proposed for the control of PM spherical actuators [9]–[11]. NNs can cope with complex dynamic systems due to their learning ability and adaptation. However, NN learning involves the modification of controller parameters rather than a control signal; in this case, large networks of nonlinear neurons are modified. These large networks require extensive training data, and they may demand a significant computational time, which limits its application for the real-time control of PM spherical actuator systems.

Manuscript received October 12, 2014; revised March 8, 2015; accepted May 26, 2015. Date of publication August 4, 2015; date of current version December 9, 2015. This work was supported by the National Natural Science Foundation of China under Project 51475033, and in part by Beijing Municipal Natural Science Foundation under Project 3152018. *(Corresponding author: Weihai Chen.)*

L. Zhang, W. Chen, and J. Liu are with the School of Automation Science and Electrical Engineering, Beihang University, Beijing 100191, China (e-mail: lzhang@buaa.edu.cn; whchen@buaa.edu.cn; jmliubuaa@126.com).

C. Wen is with the School of Electrical and Electronic Engineering, College of Engineering, Nanyang Technological University, Singapore 639798 (e-mail: ecywen@ntu.edu.sg).

Color versions of one or more of the figures in this paper are available online at http://ieeexplore.ieee.org.

Digital Object Identifier 10.1109/TIE.2015.2464186

These motivate us to develop a real-time trajectory tracking control strategy for PM spherical actuators with the ability of compensating for model uncertainties and external disturbances. One important feature in robot manipulators, assembling, and manufacturing, which involves the application of spherical actuators, is that repetitive tasks are performed over a given operation time. In addition, the electromagnetic disturbances in a PM spherical actuator periodically vary with the rotor orientation and thus have repetitive characteristics when the actuator conducts the same task repeatedly. These repetitive properties imply that an iterative learning control (ILC) is intuitively an excellent choice for PM spherical actuators to improve their trajectory tracking performance [12]–[14]. It is noted that the ILC is a learning control technique that has been successfully applied to many areas, such as industrial robots [15], [16], machining systems [17], motors [18], etc. Different from the adaptive control and NN learning, the ILC modifies the control input rather than the controller parameters since online learning is not required. The ILC can ensure convergence in just a few iterations [12]. The control input of the ILC in each run is adjusted by using the tracking error signals collected from previous runs. By doing so, high tracking performance can be achieved despite large model uncertainties and repeating disturbances.

In this paper, a new robust adaptive ILC scheme that consists of a variable-gain PD feedback control, a variable-gain PD-type ILC, and a robust control term is presented. It is a hybrid control scheme combining the advantages of an ILC algorithm, the classical PD feedback, and a robust design concept, which can cope with the model uncertainties and external disturbances, and it gives fast convergence. The PD-type ILC is a feedforward learning part for the compensation of model uncertainties and repeating disturbances. The PD feedback control part is used to speed up the convergence rate based on the current iteration errors. In addition, the gains in the PD feedback and the PD-type ILC are adapted according to the iteration times to improve the rate of convergence. Since the ILC cannot deal with nonrepetitive disturbances, in order to compensate for the random and nonrepeating noise, a robust term is designed to ensure the robustness of the controller.

The rest of this paper is organized as follows. Section II presents the torque and dynamic models of a PM spherical actuator. Section III introduces the controller design and analyzes the convergence of the control algorithm. Section IV illustrates the simulation results, and Section V presents the experiments. Finally, this paper is concluded in Section VI.

II. Dynamic and Torque Modeling

The mechanical structure of a PM spherical actuator is shown in Fig. 1. It consists of a rotor with 8 PM poles in 1 layer and a stator with 30 air-core coils in 3 layers. The rotor is supported by a passive spherical joint that contains an encoder and a two-axis tilt sensor to measure the rotor orientation.

The rotor motion is generated by the repulsion and attraction electromagnetic forces between the coils and the PM poles. By varying the current inputs of the stator coils, the desired 3-DOF motion can be achieved within the workspace (see Fig. 2). The specifications of the actuator are shown in Table I.

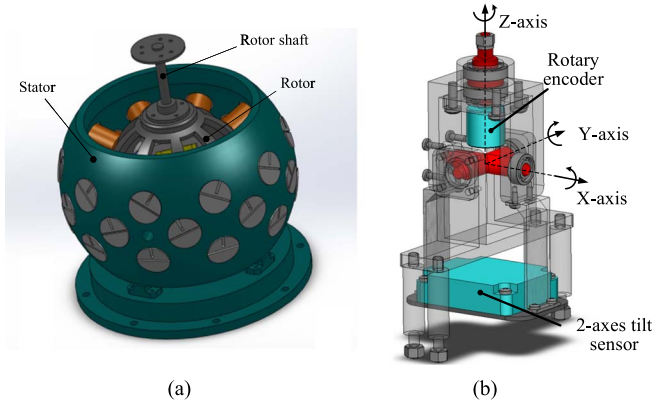

Fig. 1. Computer-aided design model. (a) Spherical actuator. (b) Passive spherical joint.

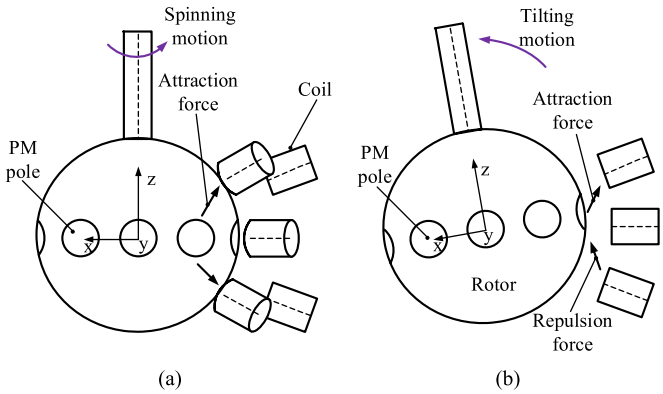

Fig. 2. Spherical actuator's 3-DOF motion. (a) Spinning motion. (b) Tilting motion.

TABLE I
Structure Specifications of the Spherical Actuator

Rotor	Number of PM poles	8 / 1 layer
	Rotor radius	57 mm
	Inner/outer rotor shell	53/58.5mm
	Cylindrical PM pole	Radius=12.5mm, Height=20mm
	Moment of rotor inertia ($kg/m^2 \times 10^{-3}$)	$J_x = 2.219$ $J_y = 2.176$ $J_z = 2.256$
Stator	Number of coils	30 / 3 layers
	Inner/outer stator shell	86/98mm
	Cylindrical coil	Radius = 11 mm, Height = 25mm
	Winding parameters	AWG 26 copper wire, 950 turns
Actuator	Rated torque	0.8Nm
	Rated power	20W
	Maximum tilting angle	±15°

A. Dynamic Modeling

Fig. 3 shows the coordinate transformation from the rotor frame to the stator frame. An XYZ Euler angle (α, β, γ) is

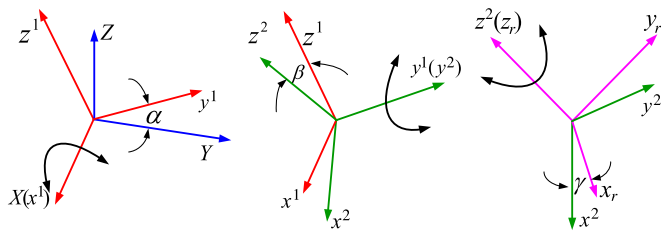

Fig. 3. Coordinate transformation.

used here to express the rotor orientation [19]. Rotation matrix R_{rs} is given by

$$R_{rs} = \begin{bmatrix} c\beta c\gamma & -c\beta s\gamma & s\beta \\ c\gamma s\alpha s\beta + c\alpha s\gamma & c\alpha c\gamma - s\alpha s\beta s\gamma & -c\beta s\alpha \\ -c\alpha c\gamma s\beta + s\alpha s\gamma & c\gamma s\alpha + c\alpha s\beta s\gamma & c\alpha c\beta \end{bmatrix} \quad (1)$$

where c and s represent the cosine and the sine, respectively.

The dynamic model of the spherical actuator is derived from Lagrange's equation, which is given by

$$M(q)\ddot{q} + C(q,\dot{q})\dot{q} + N(q,\dot{q}) = \tau_c - \tau_{d1} - \tau_{d2} - \tau_l \quad (2)$$

where $M(q)$ (shown at the bottom of the page) is the inertial matrix; $C(q,\dot{q})$ and $N(q,\dot{q})$ are the coriolis and gravity terms, respectively. $q = [\alpha \quad \beta \quad \gamma]^T$ is the Euler angle vector, and $\boldsymbol{\tau}_c = [\tau_\alpha \quad \tau_\beta \quad \tau_\gamma]^T$ is the control torque; τ_{d1} and τ_{d2} are the repetitive and nonrepetitive disturbance torque values, respectively, and τ_l is the load torque. The principal inertial moments of the rotor are $J_1 = J_{xx} = 2.219e-003\ \text{kg}\cdot\text{m}^2$, $J_2 = J_{yy} = 2.176e-003\ \text{kg}\cdot\text{m}^2$, and $J_3 = J_{zz} = 2.256e-003\ \text{kg}\cdot\text{m}^2$.

It can be seen in (2) that the rotor dynamics has a nonlinear characteristic as many interaxis coupling terms exist in the dynamic model. Note that modeling errors cannot be avoided during the dynamic modeling process. Considering the effects of the dynamic modeling uncertainties, (2) can be rewritten as

$$\widehat{M}(q)\ddot{q} + \widehat{C}(q,\dot{q})\dot{q} + \widehat{N}(q,\dot{q}) = \tau_c - \tau_{d1} - \tau_{d2} - \tau_l \quad (3)$$

where $\widehat{M}(q) = M(q) + \Delta M(q)$ is the actual inertial matrix, $\widehat{C}(q,\dot{q}) = C(q,\dot{q}) + \Delta C(q,\dot{q})$ is the actual coriolis matrix, $\widehat{N}(q,\dot{q}) = N(q,\dot{q}) + \Delta N(q,\dot{q})$ is the actual gravity matrix, and $\Delta M(q)$, $\Delta C(q,\dot{q})$, and $\Delta N(q,\dot{q})$ are the modeling errors. Let $n(\ddot{q},\dot{q},q) = \Delta M(q)\ddot{q} + \Delta C(q,\dot{q})\dot{q} + \Delta N(q,\dot{q})$; then, (3) can be shown to satisfy

$$M(q)\ddot{q} + C(q,\dot{q})\dot{q} + N(q,\dot{q}) + n(\ddot{q},\dot{q},q) = \tau_c - \tau_{d1} - \tau_{d2} - \tau_l. \quad (4)$$

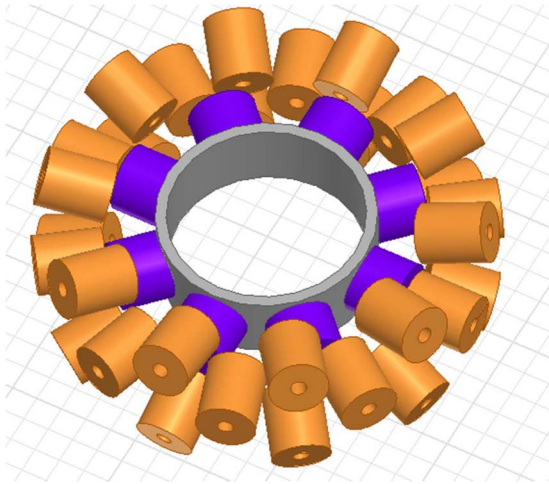

Fig. 4. FE model of the spherical actuator.

Equation (4) can be linearized along the desired trajectory $(\ddot{q}_d(t), \dot{q}_d(t), q_d(t))$ as

$$M(t)\ddot{e}(t) + (C(t) + C_1(t))\dot{e}(t) + F(t)e(t) + \vartheta(\ddot{e},\dot{e},e,t) = H(t) - \tau_c + \tau_{d1} + \tau_{d2} + \tau_l + n(t) \quad (5)$$

where $M(t) = M(q_d(t))$, $C(t) = C(q_d(t),\dot{q}_d(t))$, $\vartheta(\ddot{e},\dot{e},e,t)$ is the higher order terms, $H(t) = M(t)\ddot{q}_d(t) + C(t)\dot{q}_d(t) + N(q_d(t),\dot{q}_d(t))$, $e(t) = q_d(t) - q(t)$, $\dot{e}(t) = \dot{q}_d(t) - \dot{q}(t)$, and

$$C_1(t) = \left.\frac{\partial C}{\partial \dot{q}}\right|_{\dot{q}_d(t),q_d(t)} \dot{q}_d(t) + \left.\frac{\partial N}{\partial \dot{q}}\right|_{\dot{q}_d(t),q_d(t)}$$

$$F(t) = \left.\frac{\partial M}{\partial \dot{q}}\right|_{q_d(t)} \ddot{q}_d(t) + \left.\frac{\partial C}{\partial \dot{q}}\right|_{\dot{q}_d(t),q_d(t)} \dot{q}_d(t) + \left.\frac{\partial N}{\partial \dot{q}}\right|_{\dot{q}_d(t),q_d(t)}.$$

B. Torque Modeling

The torque model gives the relationship between the current inputs and the torque output at a specified rotor orientation. Herein, the torque of the actuator is modeled by the curve fitting of the computed data using a finite element (FE) method. The FE model established in Maxwell 3-D is shown in Fig. 4.

Since the coils are air-core coils, the torque has a linear property with respect to the current input, and the torque generated by all the coils can be calculated by summing up that of each individual coil [20]. The total torque for all the coils of the spherical actuator is

$$\mathbf{T} = [T_x \quad T_y \quad T_z]^T = \mathbf{GI} \quad (6)$$

where the torque matrix is $\mathbf{G} = [\mathbf{G}_1 \ \cdots \ \mathbf{G}_j \ \cdots \ \mathbf{G}_N]$, $\mathbf{G}_j \in \Re^{3\times 1}$ and the current input is $\mathbf{I} = [I_1 \ \cdots \ I_j \ \cdots \ I_n]^T$. $\mathbf{G}_j$ is the torque coefficient, which describes the torque contribution

$$M(q) = \begin{bmatrix} J_1c^2\beta c^2\gamma + J_2c^2\beta s^2\gamma + J_3s^2\beta & (J_1 - J_2)c\beta c\gamma s\gamma & J_3s\beta \\ (J_1 - J_2)c\beta c\gamma s\gamma & J_1s^2\gamma + J_2c^2\gamma & 0 \\ J_3s\beta & 0 & J_3 \end{bmatrix}$$

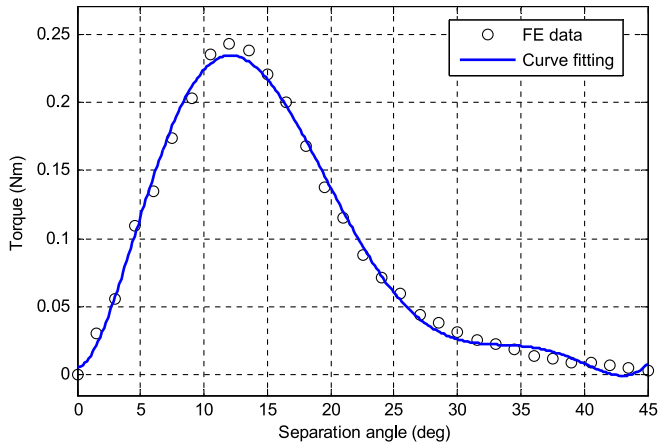

Fig. 5. Torque between a PM pole and a coil.

matrix of the jth coil. n is the number of coils, and I_j is the current input of the jth coil.

$\mathbf{G}_j$ is given as

$$\mathbf{G}_j = \begin{cases} \sum_{i=1}^{m} (-1)^{i-1} f(\varphi_{ij}) \left(\mathbf{r}_i \times \mathbf{s}_j / |\mathbf{r}_i \times \mathbf{s}_j|\right), & \text{if } \mathbf{r}_i \times \mathbf{s}_j \neq 0 \\ 0, & \text{if } \mathbf{r}_i \times \mathbf{s}_j = 0 \end{cases} \tag{7}$$

where $f(\phi_{ij})$ is the torque constant function derived by curve fitting the torque between one PM pole and one coil (see Fig. 5), and $\phi_{ij} = \cos^{-1}(\mathbf{r}_i \cdot \mathbf{s}_j)$ is the separation angle between the PM pole and the coil. It can be observed in (6) that the electromagnetic torque not only relates to the current inputs of the coils but also depends on the rotor orientation. The current inputs at a particular orientation with the required torque T are given by [21]

$$\mathbf{I} = \mathbf{G}^{\mathbf{T}} (\mathbf{G}\mathbf{G}^{\mathbf{T}})^{-1} \mathbf{T}. \tag{8}$$

It should be noted that all the coils are divided into 15 groups, and the coils whose axes are collinear are arranged into 1 group.

III. Robust Adaptive ILC Algorithm

A. Controller Design

To control the nonlinear PM spherical actuator system with uncertainties such as modeling errors, loads, and external disturbances, a new robust adaptive ILC law is developed as follows:

$$\begin{aligned} \tau_c^k(t) &= \tau_f^k(t) + \tau_{\mathrm{IL}}^k(t) + \tau_r^k(t) \\ \tau_f^k(t) &= K_{p1}^k e^k(t) + K_{d1}^k \dot{e}^k(t) \\ \tau_{\mathrm{IL}}^k(t) &= K_{p2}^k e^{k-1}(t) + K_{d2}^k e^{k-1}(t) + \tau_c^{k-1}(t) \\ \tau_r^k(t) &= \zeta \operatorname{sgn}\left(\left(\Delta\eta^{k-1}\right)^T\right) \end{aligned} \tag{9}$$

where k expresses the kth iteration with $\tau_c^k(t)\big|_{k=-1} = 0$, position tracking error $e^k(t)$ is defined as $e^k(t) = q_d(t) - q^k(t)$, $\dot{e}^k(t) = \dot{q}_d(t) - \dot{q}^k(t)$, and parameter $\eta^k(t)$ is given by

$$\eta^k(t) = \dot{e}^k(t) + \mu e^k(t). \tag{10}$$

The criterion to adjust the control gains is that the gains should become larger as the iteration progresses. Here, $e^{\lambda k}$ is selected as the control function of the gains. The adaptive control gains at the kth iteration are given by

$$\begin{cases} K_{p1}^k = e^{\lambda k} K_{p1}^0 \\ K_{d1}^k = e^{\lambda k} K_{d1}^0 \\ K_{p2}^k = e^{\lambda k} K_{p2}^0 \\ K_{d2}^k = e^{\lambda k} K_{d2}^0 \end{cases}, \quad k = 1, 2, \ldots, n \tag{11}$$

where $\lambda > 0$, and K_{p1}^0, K_{d1}^0, K_{p2}^0, and K_{d2}^0 are the initial control gains that are positive definite. Based on this design, the control gains are adjusted from iteration to iteration. In general, the tracking errors of the system are relatively large at the initial iteration, and the high gain used at this time may saturate the actuator and excite high-frequency modes. Thus, the gains during the initial iterations are small. As the iteration progresses, the system errors will be reduced, and then, a larger gain can be used to expedite the convergence rate. Therefore, the proposed control algorithm has an adaptive ability by choosing different gains in different iterations; thus, the convergence rate can be faster, and the vibration of the system can be avoided.

The proposed controller consists of three parts. As shown in (9), $\tau_f^k(t)$ is the PD feedback control term, $\tau_{\mathrm{IL}}^k(t)$ is the PD-type iterative learning term, and $\tau_r^k(t)$ is the robust control term. This hybrid control scheme can cope with the dynamic model's uncertainties and external disturbances, and it gives fast convergence. The PD feedback control part is designed to speed up the convergence rate based on the current iteration errors. The PD-type ILC is a feedforward learning part, which is designed for the compensation of the model uncertainties and repeating disturbances. The variable gains in the PD feedback control and the PD-type ILC are designed to speed up the convergence rate, and the gains are adjusted from iteration to iteration. The robust term is designed to compensate for the random and nonrepeating noise. The proposed control method combines the advantages of the ILC algorithm, the classical PD feedback, and the robust design concept, which is an original method for the control of spherical actuators.

B. Convergence Analysis

We now establish the convergence property of the tracking error that is formally stated in the following theorem.

Theorem: Consider spherical actuator system (3) under the control of controller (9) with the control gain adjusted according to (11). Then, $\lim_{k\to\infty} e^k(t) = \lim_{k\to\infty} \dot{e}^k(t) = 0$, $\forall t \in [0, T]$ holds if the controller parameters are selected based on the following conditions:

$$g_1 = \lambda_{\min}\left(K_{d1}^0 - K_{d2}^0 + 2C_1 - 2M\mu\right) > 0 \tag{12}$$

$$g_2 = \lambda_{\min}\left(\mu\left(2F + 2C\mu + \left(K_{d1}^0 - K_{d2}^0\right)\mu - 2\dot{C}_1\right)\right) > 0 \tag{13}$$

$$g_1 g_2 \geq \|F - \mu(-M\mu + C + C_1)\|_{\max}^2 \tag{14}$$

$$\zeta - \|\Delta d^k\| \geq 0 \tag{15}$$

where $\Delta d^k = d^{k+1} - d^k$, $d^k = \tau_{d2}^k - \vartheta^k$ [see (5)], parameter μ is defined in (10), $\|(\cdot)\|$ is the Euclidean norm of a matrix, and $\lambda_{\min}(\cdot)$ is the minimum eigenvalue of matrix $(\cdot)$.

Proof: First, we note that the inertia matrix $M(q)$, coriolis matrix $C(q,\dot{q})$, gravity matrix $N(q,\dot{q})$, disturbance $d(t)$, matrix $C_1(t)$, and $F(t)$ of the spherical actuator system are all bounded. In addition, there is no conflict among the conditions given in (12)–(15). Thus, control parameters K_{d1}^0, K_{d2}^0, and ζ can be easily chosen to satisfy these conditions over $[0,T]$, which can be also considered guidelines to select the design parameters.

We now define a Lyapunov function as

$$V^k = \int_0^t e^{-\rho\sigma}(\eta^k)^T \left(K_{d1}^0 + K_{d2}^0\right)\eta^k d\sigma \tag{16}$$

where ρ is a positive constant. Let $K_d^0 = K_{d1}^0 + K_{d2}^0$, and define $\Delta V^k = V^{k+1} - V^k$ and $\Delta\eta^k(t) = \eta^{k+1} - \eta^k$. Then, from (10), we can obtain

$$\begin{aligned}\Delta V^k &= \int_0^t e^{-\rho\sigma}(\eta^{k+1})^T K_d^0 \eta^{k+1} d\sigma - \int_0^t e^{-\rho\sigma}(\eta^k)^T K_d^0 \eta^k d\sigma \\ &= \int_0^t e^{-\rho\sigma}\left[(\Delta\eta^k)^T K_d^0 \Delta\eta^k + 2(\Delta\eta^k)^T K_d^0 \eta^k\right] d\sigma \\ &= \frac{1}{e^{\lambda(k+1)}}\int_0^t e^{-\rho\sigma}\left[(\Delta\eta^k)^T K_d^{k+1}\Delta\eta^k \right. \\ &\qquad \left. +2(\Delta\eta^k)^T K_d^{k+1}\eta^k\right] d\sigma. \end{aligned} \tag{17}$$

From (5), the kth and $(k+1)$th iterations can be shown to satisfy

$$\begin{aligned} &M(t)\ddot{e}^k(t) + (C(t) + C_1(t))\,\dot{e}^k(t) + F(t)e^k(t) \\ &\quad + \vartheta(\ddot{e},\dot{e},e,t)^k = H(t) - \tau_c^k + \tau_{d1} + \tau_{d2}^k + \tau_l + n(t) \end{aligned} \tag{18}$$

$$\begin{aligned} &M(t)\ddot{e}^{k+1}(t) + (C(t) + C_1(t))\,\dot{e}^{k+1}(t) + F(t)e^{k+1}(t) \\ &\quad + \vartheta(\ddot{e},\dot{e},e,t)^{k+1} = H(t) - \tau_c^{k+1} + \tau_{d1} + \tau_{d2}^{k+1} + \tau_l + n(t). \end{aligned} \tag{19}$$

Let $d^k = \tau_{d2}^k - \vartheta^k$. From (18) and (19), we have

$$\begin{aligned} &M(\ddot{e}^{k+1} - \ddot{e}^k) + (C + C_1)(\dot{e}^{k+1} - \dot{e}^k) + F(e^{k+1} - e^k) \\ &\qquad = -\left(\tau_c^{k+1} - \tau_c^k\right) + (d^{k+1} - d^k). \end{aligned} \tag{20}$$

From (10) and (20), we obtain

$$\begin{aligned} M\Delta\dot{\eta}^k &= M(\ddot{e}^{k+1} - \ddot{e}^k) + M\mu(\dot{e}^{k+1} - \dot{e}^k) \\ &= -(C + C_1)(\dot{e}^{k+1} - \dot{e}^k) - F(e^{k+1} - e^k) \\ &\quad - \left(\tau_c^{k+1} - \tau_c^k\right) + (d^{k+1} - d^k) + M\mu(\dot{e}^{k+1} - \dot{e}^k). \end{aligned} \tag{21}$$

To simplify the analysis, let $K_{p1}^0 = \mu K_{d1}^0$, and let $K_{p2}^0 = \mu K_{d2}^0$. From (9), we have

$$\begin{aligned} \tau_c^{k+1} - \tau_c^k &= K_{p1}^{k+1}e^{k+1} + K_{d1}^{k+1}\dot{e}^{k+1} + K_{p2}^{k+1}e^k \\ &\quad + K_{d2}^{k+1}e^k + \zeta\,\mathrm{sgn}\left((\Delta\eta^k)^T\right) \\ &= K_{d1}^{k+1}\eta^{k+1} + K_{d2}^{k+1}\eta^k + \zeta\mathrm{sgn}\left((\Delta\eta^k)^T\right). \end{aligned} \tag{22}$$

Substituting (22) into (21), we have

$$\begin{aligned} M\Delta\dot{\eta}^k = &-(C + C_1)(\Delta\dot{e}^k) - F\Delta e^k + M\mu(\dot{e}^{k+1} - \dot{e}^k) \\ &-\left(K_{d1}^{k+1}\eta^{k+1} + K_{d2}^{k+1}\eta^k + \zeta\,\mathrm{sgn}\left((\Delta\eta^k)^T\right)\right) + (d^{k+1} - d^k). \end{aligned} \tag{23}$$

Since $\Delta\eta^k(t) = \eta^{k+1} - \eta^k = \Delta\dot{e}^k + \mu\Delta e^k$, we have

$$\begin{aligned} M\Delta\dot{\eta}^k = &-\left(C + C_1 - M\mu + K_{d1}^{k+1}\right)\Delta\eta^k \\ &-\zeta\,\mathrm{sgn}\left((\Delta\eta^k)^T\right) - P\Delta e^k - K_d^{k+1}\eta^k + \Delta d^k \end{aligned} \tag{24}$$

where $P = F - \mu(-M\mu + C + C_1)$.

Substituting (24) into (17), we have (25), shown at the bottom of the page. Using the integration by parts, we have

$$\begin{aligned} &\int_0^t e^{-\rho\sigma}(\Delta\eta^k)^T M\Delta\dot{\eta}^k d\sigma \\ &= e^{-\rho\sigma}(\Delta\eta^k)^T M\Delta\eta^k\Big|_0^t - \int_0^t \left(e^{-\rho\sigma}(\Delta\eta^k)^T M\right)'\Delta\eta^k d\sigma \\ &= e^{-\rho t}(\Delta\eta^k)^T M\Delta\eta^k + \rho\int_0^t e^{-\rho\sigma}(\Delta\eta^k)^T M\Delta\eta^k d\sigma \\ &\quad - \int_0^t e^{-\rho\sigma}(\Delta\dot{\eta}^k)^T M\Delta\eta^k d\sigma - \int_0^t e^{-\rho\sigma}(\Delta\eta^k)^T \dot{M}\Delta\eta^k d\sigma. \end{aligned} \tag{26}$$

$$\begin{aligned} \Delta V^k &= \frac{1}{e^{\lambda(k+1)}}\int_0^t e^{-\rho\sigma}\left[(\Delta\eta^k)^T K_d^{k+1}\Delta\eta^k + 2(\Delta\eta^k)^T K_d^{k+1}\eta^k\right] d\sigma \\ &= \frac{1}{e^{\lambda(k+1)}}\left\{\int_0^t e^{-\rho\sigma}(\Delta\eta^k)^T K_d^{k+1}\Delta\eta^k d\sigma - 2\int_0^t e^{-\rho\sigma}(\Delta\eta^k)^T M\Delta\dot{\eta}^k d\sigma \right. \\ &\quad \left. -2\int_0^t e^{-\rho\sigma}(\Delta\eta^k)^T\left[\left(C + C_1 - M\mu + K_{d1}^{k+1}\right)\Delta\eta^k + P\Delta e^k + \zeta\,\mathrm{sgn}\left((\Delta\eta^k)^T\right) - \Delta d^k\right] d\sigma\right\} \end{aligned} \tag{25}$$

Since $2K_{d1}^{k+1} - K_d^{k+1} = K_{d1}^{k+1} - K_{d2}^{k+1} > K_{d1}^0 - K_{d2}^0$, substituting (26) into (25) yields, (27), shown at the bottom of the page, where $E = K_{d3}^0 + 2C_1 - 2M\mu$, $K_{d3}^0 = K_{d1}^0 - K_{d2}^0$, and

$$\begin{aligned} &2\int_0^t e^{-\rho\sigma}\mu(\Delta e^k)^T E\Delta\dot{e}^k d\sigma \\ &\quad = \mu e^{-\rho t}(\Delta e^k)^T E\Delta e^k + \rho\mu\int_0^t e^{-\rho\sigma}(\Delta e^k)^T E\Delta e^k d\sigma \\ &\qquad - \mu\int_0^t e^{-\rho\sigma}(\Delta e^k)^T(2\dot{C}_1 - 2\dot{M}\mu)\Delta e^k d\sigma. \end{aligned} \tag{28}$$

Substituting (28) into (27), we obtain (29), shown at the bottom of the page. From (12) and (13), we have

$$\begin{aligned} &-2\int_0^t e^{-\rho\sigma}(\Delta\dot{e}^k)^T P\Delta e^k d\sigma - \int_0^t e^{-\rho\sigma}(\Delta\dot{e}^k)^T E\Delta\dot{e}^k d\sigma \\ &-\int_0^t e^{-\rho\sigma}(\Delta e^k)^T\mu\left(2F + 2C\mu + K_{d3}^0\mu - 2\dot{C}_1\mu\right)\Delta e^k d\sigma \\ &\quad \le -\int_0^t e^{-\rho\sigma}\left(g_1\|\Delta\dot{e}\|^2 + 2(\Delta\dot{e}^k)^T P\Delta e^k + g_2\|\Delta e\|^2\right)d\sigma. \end{aligned} \tag{30}$$

Since

$$\begin{aligned} &(\Delta\dot{e}^k)^T\left(F - \mu(-M\mu + C + C_1)\right)\Delta e^k \\ &\quad \ge -\left\|\Delta\dot{e}^k\right\| * \|F - \mu(-M\mu + C + C_1)\|_{\max} * \|\Delta e^k\| \end{aligned}$$

from (14), we can obtain

$$-\int_0^t e^{-\rho\sigma}\left(g_1\|\Delta\dot{e}\|^2 + 2(\Delta\dot{e}^k)^T P\Delta e^k + g_2\|\Delta e\|^2\right)d\sigma \le 0. \tag{31}$$

Since $(\Delta\eta^k)^T\Delta d^k \le \left\|(\Delta\eta^k)^T\right\| * \left\|\Delta d^k\right\|$, which is based on (15), we can obtain

$$\begin{aligned} &(\Delta\eta^k)^T\left(\zeta\,\mathrm{sgn}\left((\Delta\eta^k)^T\right) - \Delta d^k\right) \\ &\qquad \ge \left(\zeta - \|\Delta d^k\|\right)\left\|(\Delta\eta^k)^T\right\| \ge 0. \end{aligned} \tag{32}$$

From (29)–(32), we have

$$\Delta V^k < 0, \quad \text{i.e.,} \quad V^{j+1} < V^j.$$

Because K_{d1}^0 and K_{d2}^0 are positive-definite matrices, when $k \to \infty$, $\eta^k(t) \to 0$. From the definition of $\eta^k(t)$ in (10), we can obtain that

$$\lim_{k\to\infty} e^k(t) = \lim_{k\to\infty}\dot{e}^k(t) = 0 \qquad \forall t \in [0, T].$$

Thus, the tracking errors converge to zero as the number of iterations approaches infinity, i.e., the convergence property of the control algorithm can be ensured.

IV. Simulations

To evaluate the effectiveness and robustness of the proposed control algorithm, simulations are carried out in this section. First, the simulation is to investigate how the effects of modeling uncertainties and external repetitive and nonrepetitive disturbances are compensated for. Then, in consideration of payload influences in practical applications, different payloads are simulated to observe their respective tracking performance.

$$\begin{aligned} \Delta V^k < \frac{1}{e^{\lambda(k+1)}}\Bigg\{ &-e^{-\rho t}(\Delta\eta^k)^T M\Delta\eta^k - \rho\int_0^t e^{-\rho\sigma}(\Delta\eta^k)^T M\Delta\eta^k d\sigma - 2\int_0^t e^{-\rho\sigma}(\Delta\dot{e}^k)^T P\Delta e^k d\sigma \\ &- 2\int_0^t e^{-\rho\sigma}\mu(\Delta e^k)^T P\Delta e^k d\sigma - \int_0^t e^{-\rho\sigma}(\Delta\dot{e}^k)^T E\Delta\dot{e}^k d\sigma - 2\int_0^t e^{-\rho\sigma}\mu(\Delta e^k)^T E\Delta\dot{e}^k d\sigma \\ &-\mu^2\int_0^t e^{-\rho\sigma}(\Delta e^k)^T E\Delta e^k d\sigma - 2\int_0^t e^{-\rho\sigma}(\Delta\eta^k)^T\left[\zeta\,\mathrm{sgn}\left((\Delta\eta^k)^T\right) - \Delta d^k\right]d\sigma\Bigg\} \end{aligned} \tag{27}$$

$$\begin{aligned} \Delta V^k < \frac{1}{e^{\lambda(k+1)}}\Bigg\{ &-e^{-\rho t}(\Delta\eta^k)^T M\Delta\eta^k - \rho\int_0^t e^{-\rho\sigma}(\Delta\eta^k)^T M\Delta\eta^k d\sigma - 2\int_0^t e^{-\rho\sigma}(\Delta\dot{e}^k)^T P\Delta e^k d\sigma \\ &- \rho\mu\int_0^t e^{-\rho\sigma}(\Delta e^k)^T E\Delta e^k d\sigma - \int_0^t e^{-\rho\sigma}(\Delta e^k)^T\mu\left(2F + 2C\mu + K_{d3}^0\mu - 2\dot{C}_1\right)\Delta e^k d\sigma \\ &- \int_0^t e^{-\rho\sigma}(\Delta\dot{e}^k)^T E\Delta\dot{e}^k d\sigma - \mu e^{-\rho t}(\Delta e^k)^T E\Delta e^k - 2\int_0^t e^{-\rho\sigma}(\Delta\eta^k)^T\left(\zeta\mathrm{sgn}\left((\Delta\eta^k)^T\right) - \Delta d^k\right)d\sigma\Bigg\} \end{aligned} \tag{29}$$

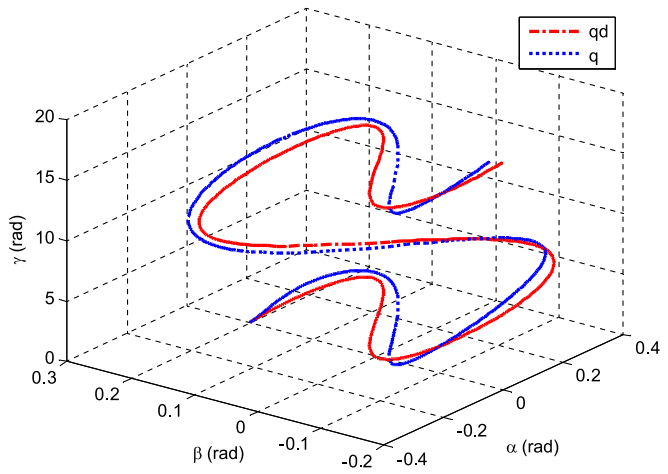

Fig. 6. Three-DOF trajectory tracking with the PD control.

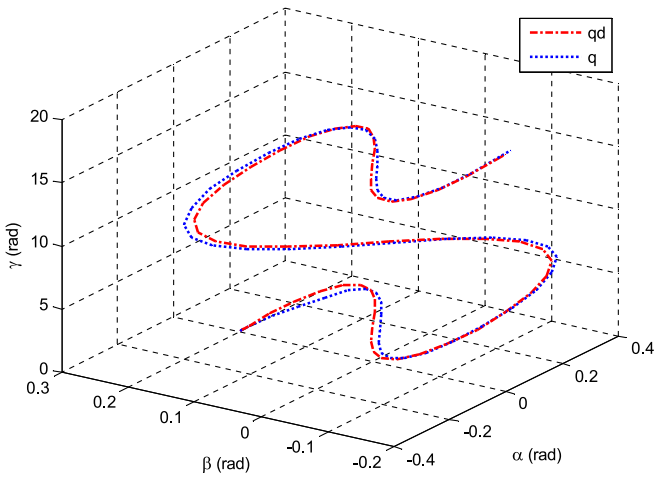

Fig. 7. Three-DOF trajectory tracking with the computed torque control method.

A. Trajectory Tracking in Presence of Modeling Errors and Random Disturbances

The desired trajectory is

$$q(t) = \begin{bmatrix} q_1(t) \\ q_2(t) \\ q_3(t) \end{bmatrix} = \begin{bmatrix} \left(\frac{\pi}{12}\right) * \sin(2\pi t) \\ 0.2 * \cos(\pi t) \\ 2\pi t \end{bmatrix}, \quad t \in [0, 3].$$

The modeling errors are set as follows:

$$\Delta M(q) = 0.2 * M(q), \quad \Delta C(q, \dot{q}) = 0.2 * C(q, \dot{q})$$
$$\Delta G(q, \dot{q}) = [0.002; 0.001; 0.001].$$

The random external disturbance torque is set as

$$\tau_d = r * [\cos(\pi t), \exp(-\pi t), \sin(2\pi t)]$$

where $r = 0.02$ is randomly distributed in $(-0.02, 0.02)$ (in newton meters). The controller gain matrices are $K_{p1}^0 = \text{diag}[1, 1, 1]$ and $K_{p2}^0 = \text{diag}[0.2, 0.2, 0.2]$, and the gain updating parameter λ is chosen as $\lambda = 0.5$. The gains of the PD controller are the same as the gains of the PD term in the proposed controller before the iteration process started. The computed torque control law is given by

$$\tau_c = M(q)(\ddot{q}_d + K_v\dot{e} + K_p e) + C(q, \dot{q})\dot{q}.$$

The controller gain matrices of the computed torque control law are $K_p = \text{diag}[350, 350, 350]$ and $K_v = \text{diag}[20, 20, 20]$. They are selected based on the dynamic characteristic of the spherical actuator system under the control law.

Figs. 6 and 7 show the trajectory tracking performance under the PD control method and the computed torque control method, respectively. q denotes the actual output, and q_d is the desired trajectory. The maximum position tracking errors during the motion are about 0.05 rad under the PD control and 0.04 rad under the computed torque control, which are too large and are not acceptable for PM spherical actuators. Although the same system is under the control of the proposed algorithm, the tracking performance at the fourth iteration is shown in Fig. 8. It can be observed that the actual trajectory fits the desired trajectory well, and the maximum position tracking error during the motion is smaller than 0.001 rad. The results

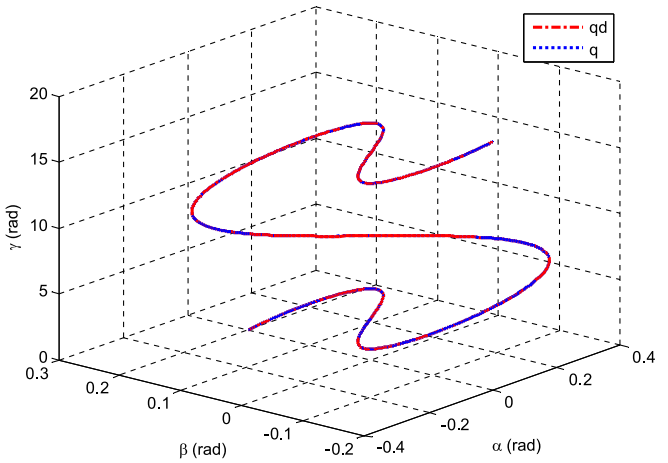

Fig. 8. Three-DOF trajectory tracking with the proposed algorithm.

show that, compared with the PD control and computed torque control methods, the proposed algorithm can give much better performance in the presence of model uncertainties and random nonrepetitive external disturbances, verifying the effectiveness and robustness of the proposed algorithm.

B. Trajectory Tracking in Presence of Modeling Errors and Load

In consideration of the load effect in practical applications, both the load and the modeling errors are now considered. The desired trajectory, the modeling errors, and the control parameters are the same as those in Section IV-A. The load is set as $\tau_l = [0.05; 0.05; 0.2]$.

The tracking performance under the PD and computed torque control methods is shown in Figs. 9 and 10, respectively. We can see that there is a steady-state tracking error during the motion under the control of both the PD control and computed torque control methods, which means that the model uncertainty and the load seriously affect the accuracy performance. However, under the proposed method, we can see that the desired trajectory is closely tracked at the fourth iteration in Fig. 11. The maximum position tracking errors of three Euler angles α, β, and γ are smaller than 0.0004, 0.0001, and 0.0001 rad, respectively.

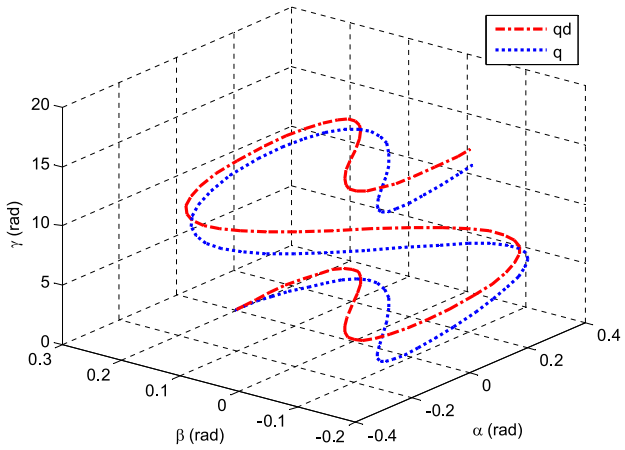

Fig. 9. Trajectory tracking under the PD control with model uncertainties and the load.

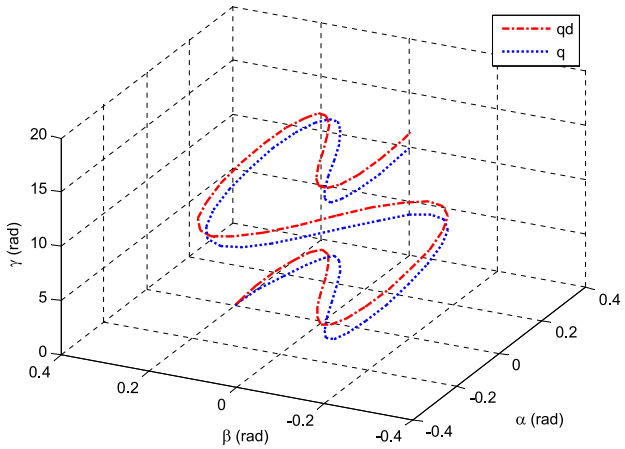

Fig. 10. Trajectory tracking under the computed torque control method with model uncertainties and the load.

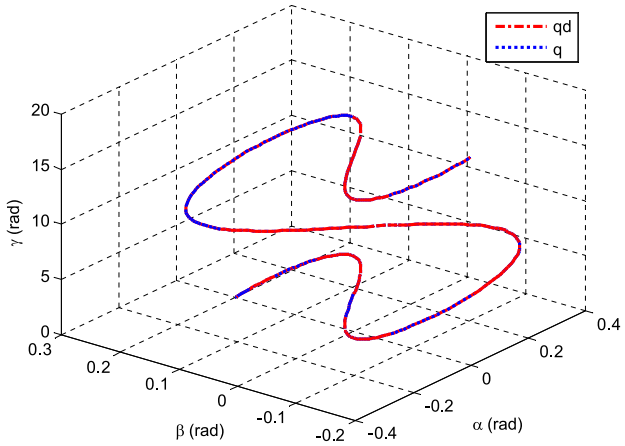

Fig. 11. Trajectory tracking under the proposed control algorithm with model uncertainties and the load.

In Fig. 12, we can observe that, at the beginning, the Euclidean norms of the three Euler angles' position errors are (0.4544, 0.4667, 1.6832) (in radians). However, after four iterations, the position errors are reduced to about (0.0008, 0.0004, 0.0011) (in radians). These results again demonstrate that the proposed algorithm can greatly improve the tracking performance under the influence of modeling errors and the payload.

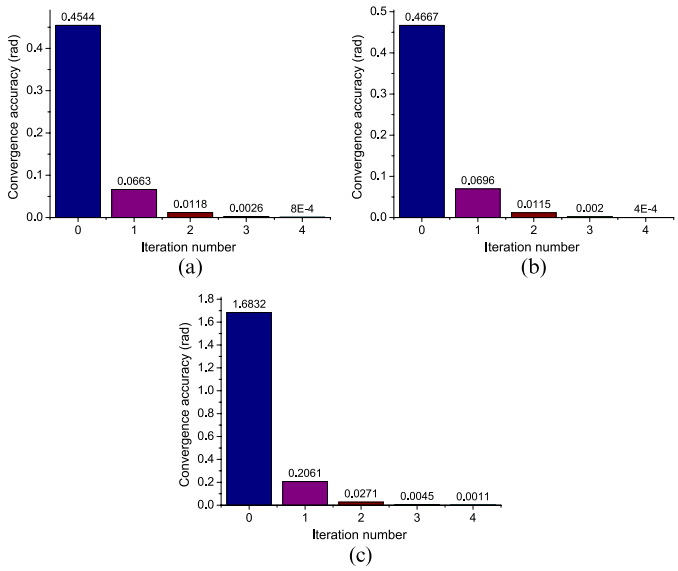

Fig. 12. Position convergence accuracy during the iterative procedure. (a) α angle. (b) β angle. (c) γ angle.

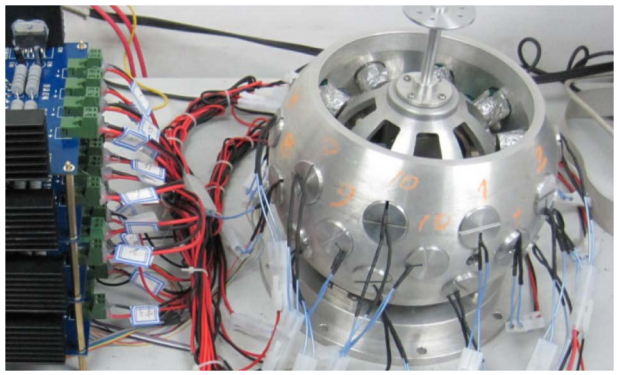

Fig. 13. Experimental prototype.

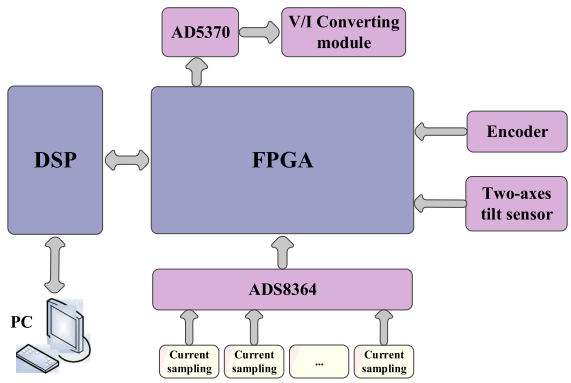

Fig. 14. Diagram of the control system.

V. Experimental Evaluation

Fig. 13 shows the experimental prototype of the spherical actuator. The rotor is connected to the stator through a passive spherical joint, which contains an encoder and a two-axis tilt sensor. A block diagram of the control system is shown in Fig. 14, which contains a PC, DSP TMS320F28335, a field-programmable gate array (FPGA), a $V-I$ converting module, an orientation and current measurement module, etc. A friendly graphical user interface program written with VC++ is

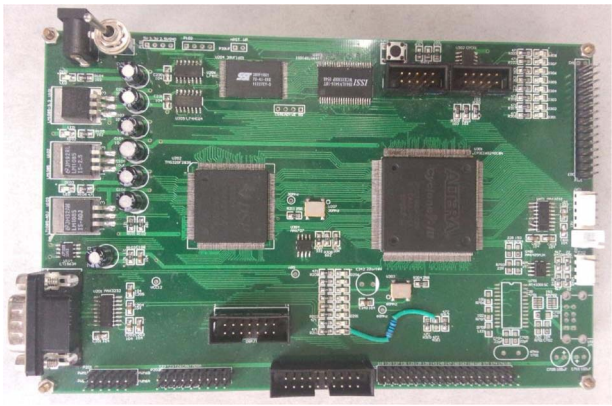

Fig. 15. Core control module.

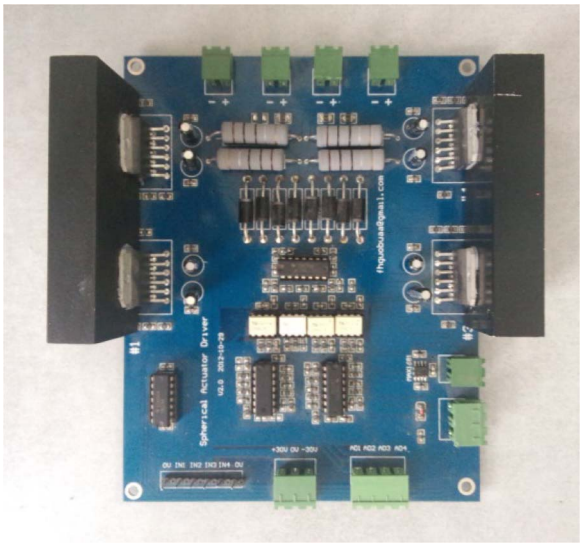

Fig. 16. $V-I$ converting and current sampling module.

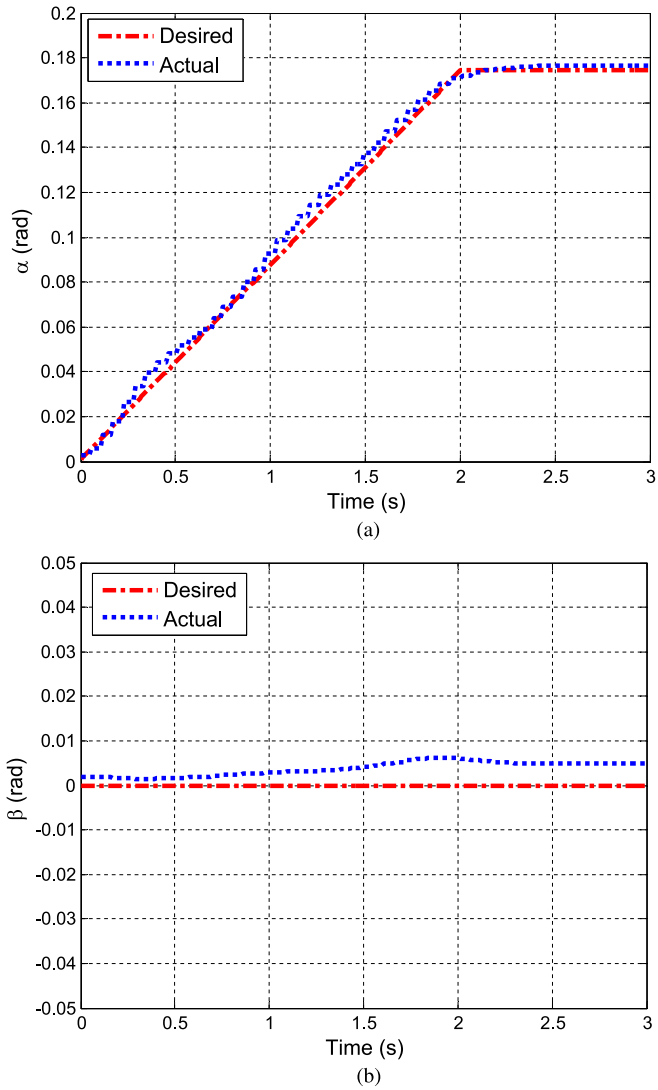

Fig. 17. Experimental results under the PD control. (a) α angle. (b) β angle.

developed on the PC in the VS2010 environment, through which the control mode selection, control parameter setting, command sending, and status displaying can be easily done.

As shown in Fig. 15, the DSP and the FPGA comprise the core control module. The maximum clock frequency of the DSP is 150 MHz, which is in charge of task scheduling, algorithm computing, and communicating with the PC. The FPGA is responsible for driver function programming and for receiving and processing the sensor information. To simultaneously provide a multichannel and bipolar current, the digital-to-analog (D/A) chip AD5370 that can offer 40 channels with 16-bit-resolution D/A converting is used. Fig. 16 shows the $V-I$ converting and current sampling module. The $V-I$ converting module is responsible for providing the power current to the coils. OPA549 is utilized to complete the $V-I$ converting based on the signals from AD5370.

To observe the control performance simply, a typical trajectory along the x-axis of the rotor is conducted. In the experiment, a load is fixed to the output shaft, and the mass of the load is about 0.2 kg. The rotor is controlled to move along the desired trajectory $q(t) = [(\pi/36) * t, 0, 0]$, $t \in [0, 2]$, and then, it stays at orientation $[\pi/18, 0, 0]$. The controller gain matrices are $K_{p1}^0 = \text{diag}[1.2, 1.2, 1.2]$ and $K_{p2}^0 = \text{diag}[0.2, 0.2, 0.2]$. Parameter λ for updating the control gains is selected to be $\lambda = 0.5$.

The orientation control frequency of the control system is 50 Hz. Figs. 17 and 18 show the control performance under the PD control and computed torque control methods, respectively. It can be seen that, under both the PD and computed torque control methods, an undesirable dynamic response occurs, with the maximum tracking error being about 0.5°. This denotes that the control accuracy of the PD control and computed torque control methods is affected by the modeling uncertainties and disturbances in the actual system. Fig. 19 shows the experimental results at the third iteration under the proposed control algorithm. It can be observed that the actual trajectory fits the desired trajectory well, and the maximum tracking error is only about 0.1°, which indicates that the uncertainties and disturbances in the practical system are effectively compensated for. The position convergence accuracy during the iterative procedure is shown in Fig. 20, where we can observe that, at the beginning, the Euclidean norms of the α and β angles are 0.0664 and 0.0667 rad, respectively, whereas after three iterations,

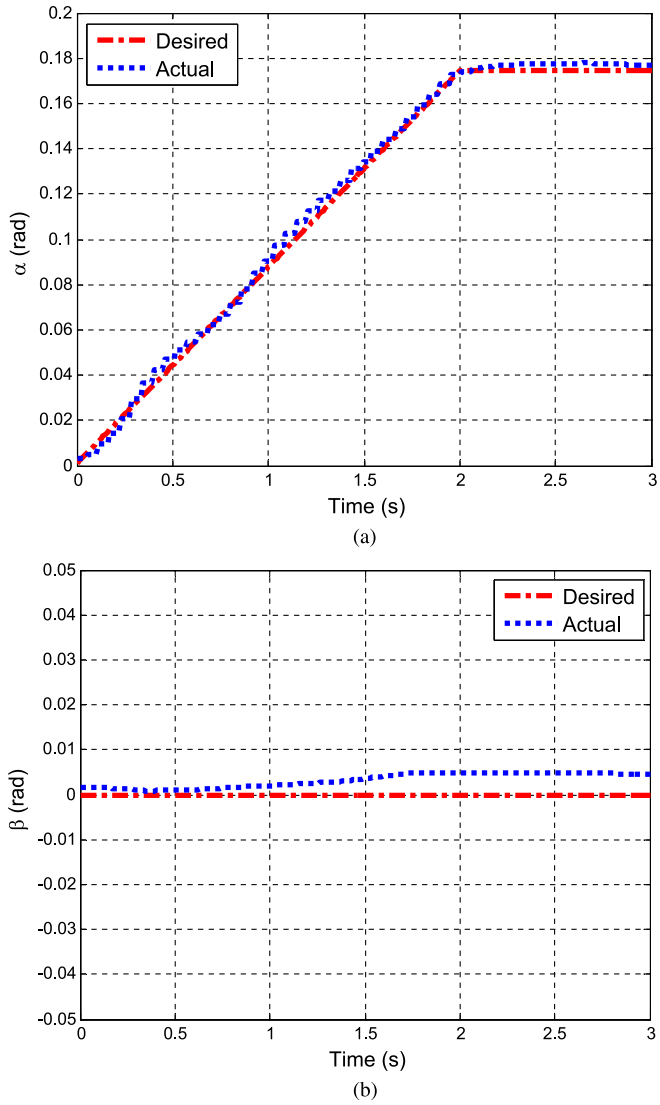

Fig. 18. Experimental results under the computed torque control method. (a) α angle. (b) β angle.

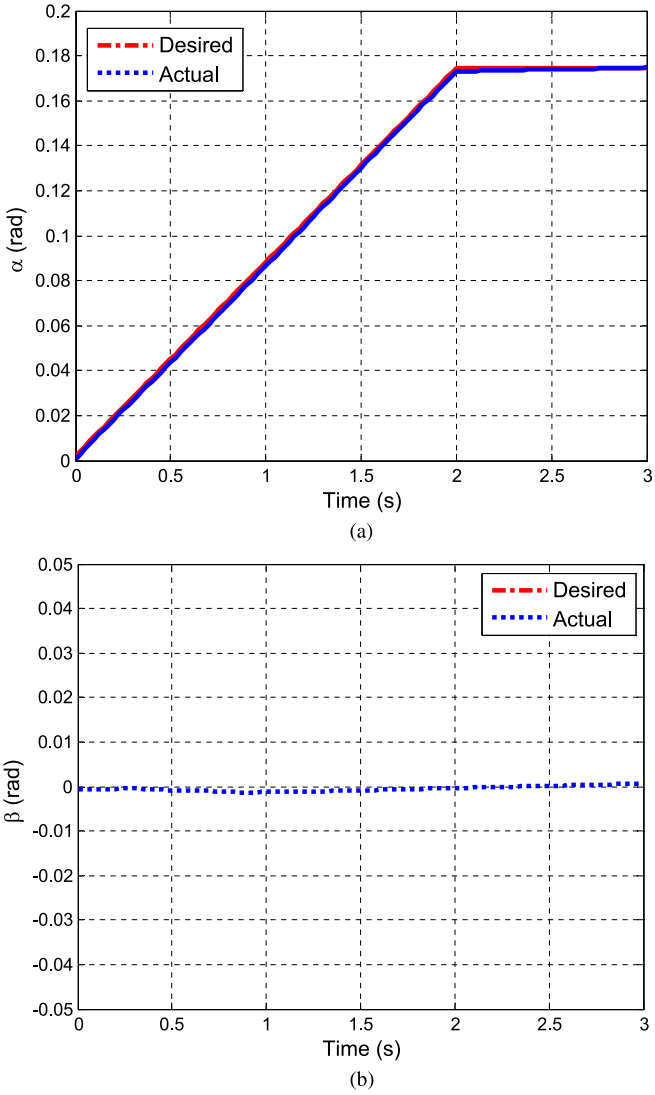

Fig. 19. Experimental results under the proposed control algorithm. (a) α angle. (b) β angle.

the Euclidean norms of the α and β angles are reduced to 0.0182 and 0.0119 rad, respectively. We can see that the control accuracy of the actuator is improved with the increase in the iteration numbers. The experimental results show that, compared with the PD control and computed torque control methods, the proposed control algorithm can give much better performance in actual systems, demonstrating the effectiveness of the proposed algorithm.

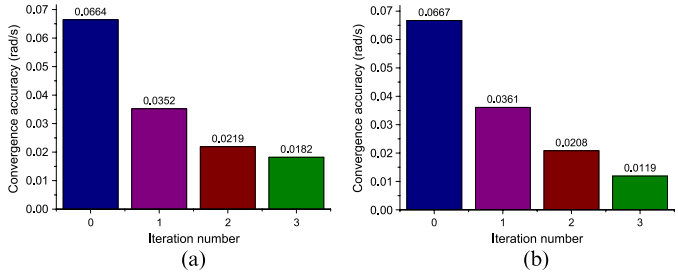

Fig. 20. Position convergence accuracy during the iterative procedure. (a) α angle. (b) β angle.

VI. Conclusion

This paper has investigated the trajectory tracking control of PM spherical actuators in the presence of uncertainties such as modeling errors, a load, and external disturbances. Nonlinear dynamic models with uncertainties have been established based on Lagrange's equations, and a torque model has been formulated by FE analysis and a curve fitting method. To compensate for the effects of nonlinearities and uncertainties on the trajectory tracking performance, a new hybrid control scheme combining the advantages of an ILC algorithm, the classical PD feedback, and a robust design concept has been proposed. The convergence of tracking errors is theoretically established. The simulation results have shown that the proposed algorithm can effectively deal with the modeling uncertainties and external disturbances, and it can achieve fast convergence. An experimental platform that consists of a spherical actuator and its control system has been developed. The experimental results have also verified the validity of the proposed algorithm to handle an actual system.

REFERENCES

[1] L. Yan, I. M. Chen, C. K. Lim, G. L. Yang, and K. M. Lee "Modeling, design and experimental investigation on electromagnetic spherical actuators," in *Mechanisms and Machine Science*, vol. 4. Berlin, Germany: Springer-Verlag, 2011.

[2] J. Hey, T. J. Teo, V. P. Bui, G. Yang, and R. Martinez-Botas, "Electromagnetic actuator design analysis using a two-stage optimization method with coarse-fine model output space mapping," *IEEE Trans. Ind. Electron.*, vol. 61, no. 10, pp. 5453–5464, Oct. 2014.

[3] H. Son and K.-M. Lee, "Open-loop controller design and dynamic characteristics of a spherical wheel motor," *IEEE Trans. Ind. Electron.*, vol. 57, no. 10, pp. 3475–3482, Oct. 2010.

[4] K. Bai and K.-M. Lee, "Direct field-feedback control of a ball-joint-like permanent-magnet spherical motor," *IEEE/ASME Trans. Mechatronics*, vol. 19, no. 3, pp. 975–986, Jun. 2014.

[5] S. Maeda, K. Hirata, S. Ikejiri, and M. Tong, "Feedback control of electromagnetic spherical actuator with three-degree-of-freedom," in *Proc. ICEM*, Rome, Italy, Sep. 2010, pp. 1–6.

[6] H. Son and K.-M. Lee, "Control system design and input shape for orientation of spherical wheel motor," *Control Eng. Pract.*, vol. 24, pp. 120–128, Mar. 2014.

[7] W. Wang, J. Wang, G. W. Jewell, and D. Howe, "Design and control of a novel spherical permanent magnet actuator with three degree of freedom," *IEEE/ASME Trans. Mechatronics*, vol. 8, no. 4, pp. 457–468, Dec. 2003.

[8] K. M. Lee, R. B. Roth, and Z. Zhou, "Dynamic modeling and control of a ball-joint-like variable-reluctance spherical motor," *Trans. ASME, J. Dyn. Syst. Meas. Control*, vol. 118, no. 1, pp. 29–40, Mar. 1996.

[9] C. Xia, C. Guo, and T. Shi, "A neural-network-identifier and fuzzy-controller-based algorithm for dynamic decoupling control of permanent-magnet spherical motor," *IEEE Trans. Ind. Electron.*, vol. 57, no. 8, pp. 2868–2878, Aug. 2010

[10] Z. Li, "Robust control of PM spherical stepper motor based on neural networks," *IEEE Trans. Ind. Electron.*, vol. 56, no. 8, pp. 2945–2954, Aug. 2009.

[11] C. Junghyun, N. Niguchi, and K. Hirata, "Feedback control of outer rotor spherical actuator using adaptive neuro-fuzzy inference system," in *Proc. 7th ICST*, 2013, pp. 401–405.

[12] D. A. Bristow, M. Tharayil, and A. G. Alleyne,"A survey of iterative learning control," *IEEE Control Syst. Mag.*, vol. 26, no. 3, pp. 96–114, Jun. 2006.

[13] Y. Zhao, Y. Lin, F. Xi, and S. Guo, "Calibration-based iterative learning control for path tracking of industrial robots," *IEEE Trans. Ind. Electron.*, vol. 62, no. 5, pp. 2921–2929, May 2015.

[14] D. Huang, J.-X. Xu, V. Venkataramanan, and T. C. T. Huynh, "High-performance tracking of piezoelectric positioning stage using current-cycle iterative learning control with gain scheduling," *IEEE Trans. Ind. Electron.*, vol. 61, no. 2, pp. 1085–1098, Feb. 2014.

[15] P. R. Ouyang, W. J. Zhang, and M. M. Gupta, "An adaptive switching learning control method for trajectory tracking of robot manipulators," *Mechatronics*, vol. 16, no. 1, pp. 51–61, Feb. 2006.

[16] C. T. Freeman and Y. Tan, "Iterative learning control with mixed constraints for point-to-point tracking," *IEEE Trans. Control Syst. Technol.*, vol. 21, no. 3, pp. 604–616, May 2013.

[17] Z. Wang, A. Witthauer, Q. Zou, and G.-Y. Kim, "Control of a magnetostrictive-actuator-based micromachining system for optimal high-speed microforming process," *IEEE/ASME Trans. Mechatronics*, vol. 20, no. 3, pp. 1046–1055, Jun. 2015.

[18] A. Mohammadpour, S. Mishra, and L. Parsa, "Iterative learning control for fault-tolerance in multi-phase permanent-magnet machines," in *Proc. ACC*, Washington, DC, USA, Jun. 2013, pp. 5929–5934.

[19] R. M. Murray, Z. X. Li, and S. S. Sastry, *A Mathematical Introduction to Robotic Manipulation*. Boca Raton, FL, USA: CRC Press, 1994

[20] C. K. Lim, I.-M. Chen, L. Yan, G. Yang, and K.-M. Lee, "Electromechanical modeling of a permanent-magnet spherical actuator based on magnetic-dipole-moment principle," *IEEE Trans. Ind. Electron.*, vol. 56, no. 5, pp. 1640–1648, May 2009.

[21] L. Zhang, W. Chen, L. Yan and J. Liu, "Trajectory planning and current control optimization of three DOF spherical actuator," in *Proc. IEEE/RSJ IROS*, San Francisco, CA, USA, Sep. 2011, pp. 744–749.

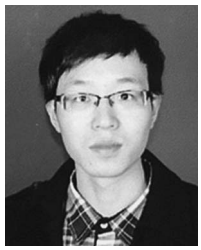

Liang Zhang received the B.S. degree from Zhengzhou University, Zhengzhou, China, in 2009. He is currently working toward the Ph.D. degree in the School of Automation Science and Electrical Engineering, Beihang University, Beijing, China.

His current research interests include robots, control, and navigation systems.

Weihai Chen (M'00) received the B.S. degree from Zhejiang University, Hangzhou, China, in 1982 and the M.S. and Ph.D. degrees from Beihang University, Beijing, China, in 1988 and 1996, respectively.

He is currently a Professor with the School of Automation Science and Electrical Engineering, Beihang University. His current research interests include modular robots, actuators, automation, and control.

Jingmeng Liu received the B.S. degree from Anhui Polytechnic University, Wuhu, China, in 1991 and the M.S. and Ph.D. degrees from Beihang University, Beijing, China, in 2000 and 2004, respectively.

He is currently an Associate Professor with the School of Automation Science and Electrical Engineering, Beihang University. His current research interests include actuators, precision control, and mechatronics.

Changyun Wen (F'10) received the B.Eng. degree from Xi'an Jiaotong University, Xi'an, China, in July 1983 and the Ph.D. degree from The University of Newcastle, Callaghan, Australia, in February 1990.

From August 1989 to August 1991, he was a Postdoctoral Fellow with The University of Adelaide, Adelaide, Australia. Since August 1991, he has been with the School of Electrical and Electronic Engineering, College of Engineering, Nanyang Technological University, Singapore, where he is currently a Professor. His main research activities include the areas of adaptive control, the development of battery management systems, ejector-based air-conditioning systems, switching and impulsive systems, system identification, the control and synchronization of chaotic systems, and biomedical signal processing.

Dr. Wen is an Associate Editor of a number of journals. He was a member of the 2011 IEEE Fellows Committee and is a Distinguished Lecturer of the IEEE Control Systems Society.